ORIGINAL ARTICLE

Enhancing immunotherapy efficacy against MHC-I deficient triple-negative breast cancer using LCL161-loaded macrophage membrane-decorated nanoparticles

Wen Zhang[a,b], Yihui Zhai[b,g], Ying Cai[b,g], Xiang Gong[a,b], Yunxuan Jiang[d], Rong Rong[e], Chao Zheng[a,b], Binyu Zhu[b,g], Helen He Zhu[f], Hao Wang[a,*], Yaping Li[b,d,e,*], Pengcheng Zhang[c,*]

[a]China State Institute of Pharmaceutical Industry, Shanghai 201203, China
[b]State Key Laboratory of Drug Research & Center of Pharmaceutics, Shanghai Institute of Materia Medica, Chinese Academy of Sciences, Shanghai 201203, China
[c]School of Biomedical Engineering & State Key Laboratory of Advanced Medical Materials and Devices, ShanghaiTech University, Shanghai 201210, China
[d]School of Chinese Materia Medica, Nanjing University of Chinese Medicine, Nanjing 210023, China
[e]Yantai Institute of Materia Medica, Shandong 264000, China
[f]State Key Laboratory of Oncogenes and Related Genes, Renji-Med-X Stem Cell Research Center, Department of Urology, Ren Ji Hospital, School of Medicine and School of Biomedical Engineering, Shanghai Jiao Tong University, Shanghai 200127, China
[g]University of Chinese Academy of Sciences, Beijing 100049, China

Abstract Current cytotoxic T lymphocyte (CTL) activating immunotherapy requires a major histocompatibility complex I (MHC-I)-mediated presentation of tumor-associated antigens, which malfunctions in around half of patients with triple-negative breast cancer (TNBC). Here, we create a LCL161-loaded macrophage membrane decorated nanoparticle (LMN) for immunotherapy of MHC-I-deficient TNBC. SIRPα on the macrophage membrane helps LMNs recognize CD47-expressing cancer cells for targeted delivery of LCL161, which induces the release of high mobility group protein 1 and proinflammatory cytokines from cancer cells. The released cytokines and high mobility group protein 1 activate antitumor immunity by increasing the intratumoral density of the phagocytic macrophage subtype by 15 times and

Immune checkpoint;
Innate immunity

elevating the intratumoral concentration of CTL lymphotoxin by 4.6 folds. LMNs also block CD47-mediated phagocytosis suppression. LMNs inhibit the growth of MHC-I-deficient TNBC tumors, as well as those resistant to combined therapy of anti-PDL1 antibody and albumin-bound paclitaxel, and prolong the survival of animals, during which process CTLs also play important roles. This macrophage membrane-decorated nanoparticle presents a generalizable platform for increasing macrophage-mediated antitumor immunity for effective immunotherapy of MHC-I-deficient cancers.

1. Introduction

Cancer immunotherapy has transformed the treatment of many types of cancer including triple-negative breast cancer (TNBC), mainly by modulating acquired immunity[1−3]. While effective, the response rate is only 20%−40%[4], and many patients relapse after remission[5,6]. Current immunotherapy such as immune checkpoint blockade (ICB) therapy usually requires a sufficient intratumoral infiltration of cytotoxic T lymphocytes (CTLs). For tumors with relatively low intratumoral CTLs such as TNBC, a combination use of chemotherapy with ICB is necessary in the clinic[7]. Combinatorial therapy with ICB and molecular-targeted drugs or cytokines has also been explored in both preclinical and clinical settings[8−14]. These treatments are capable of inducing immunogenic cell death (ICD) of cancer cells and reversing the immunosuppressive microenvironment to restore functional CD8$^+$ T cells in tumors. However, the efficacy of the treatments is not satisfactory, mainly due to a deficiency in the neoantigen presentation that is essential for CTL-mediated immune clearance[6,15−17].

A lack of the major histocompatibility complex class I (MHC-I) is one of the main causes of the malfunction of the antigen presentation by cancer cells[18,19]. Loss of MHC-I expression is observed in approximately 40%−60% of some cancers, including large B-cell lymphoma, non-small cell lung cancer, and TNBC[20−22], and is associated with poor prognosis and metastases of many types of cancer[23]. For instance, patients with a higher expression of MHC-I showed a longer progression-free survival than those with low expression of MHC-I after combination therapy with carboplatin and atezolizumab in a randomized phase II clinical trial[24]. MHC-I malfunction is a result of molecular changes from genetic to post-translational levels. Downregulation of MHC-I caused by cytokine deficiency or promotion of MHC-I degradation during treatment can be pharmacologically restored[25]. However, genetic deletion of β2-microglobulin (β2M) or related genes comprising MHC-I in cancer cells is irreversible[16,25], leading to immune evasion to CTL-mediated clearance. Thus, chimeric antigen receptor (CAR) T-cell (CAR-T) has been explored, which can kill cancer cells in an MHC-I-independent manner[26]. Nevertheless, it is still challenging to identify the tumor-specific surface antigen for the design of CAR, and the immunosuppressive microenvironment and the possible severe cytokine release syndrome (CRS) also hinder its application in the treatment of solid tumors such as TNBC[27−29]. Therefore, a new strategy is required to improve the therapeutic efficacy of MHC-I-deficient tumors.

Loss of MHC-I may activate innate immunity-mediated cancer clearance[24,30]. Natural killer (NK) cells and macrophages are two major types of innate immune cells that can eradicate cancer cells in an MHC-I-independent way. To improve the specificity of these cells, CAR-NK and CAR-macrophage have been developed for the treatment of solid tumors as a complement or alternative to CAR-T therapy[31]. The activities of these natural and engineered innate immune cells are hindered by phagocytosis checkpoints such as CD47-SIRPα[32−34], and high expression of CD47 is positively associated with a poor prognosis in patients with TNBC[35,36]. However, blocking CD47 with antibodies is unsuccessful in clinical trials because of obvious side effects, probably due to the high abundance of CD47 in normal cells especially erythrocytes, and its high affinity for antibodies. As a result, while enhancing macrophage tumor phagocytosis, anti-CD47 antibodies can cause erythrocyte phagocytosis resulting in erythrocyte agglutination and rupture[33,37]. Therefore, other strategies are still needed to improve phagocytic checkpoint blockade while reducing toxicity.

The loss of MHC-I is observed in 59% of patients with TNBC (pharmacologically irreversible in half of them), who respond poorly to current ICB therapy[22,24]. Our previous study showed that transcriptionally silenced MHC-I expression of TNBC cells could be rescued by epigenetic therapy, but the same treatment was ineffective in TNBC with β2M gene deletion[25]. Here, we report a LCL161-loaded macrophage membrane-decorated nanoparticle (LMN) with membrane-disrupting activity-caged M70 peptide for the treatment of TNBC with β2M gene deletion (Fig. 1A). We hypothesized that the SIRPα on LMNs would recognize CD47 expressed on 4T1$^{\text{H-2Kb KO}}$ cells, which interaction would facilitate cellular uptake of LMNs by cancer cells. The SIRPα on LMNs would also compete with SIRPα on macrophage for CD47 on 4T1$^{\text{H-2Kb KO}}$ cells, and thus unleash CD47-mediated phagocytosis inhibition[38]. The LMNs were then expected to deshell after the membrane-disrupting activity of M70 was resumed in an intracellular reductive environment and to release LCL161 (an antagonist of cellular inhibition of apoptosis proteins 1 and 2 (cIAP1/2)), which could trigger ICD at high concentration and more importantly activate noncanonical NF-κB pathway to upregulate the expression of multiple inflammatory factors at a nonlethal concentration[16,39]. These factors could induce phagocytic macrophage subtype formation and dendritic cell (DC) maturation, and the latter would activate CTLs and their lymphotoxin secretion, which could promote cancer cell phagocytosis by macrophages (Fig. 1B). The LMNs were expected to improve the outcome of model mice bearing orthotopic 4T1$^{\text{H-2Kb KO}}$ tumors or 4T1 tumors refractory to chemoimmunotherapy. Unlike current antitumor immunotherapies (such as immune checkpoint inhibitors) that focus on increasing CD8$^+$ T cell activity, LMNs aim to activate macrophage phagocytosis of MHC-I deficient cancer
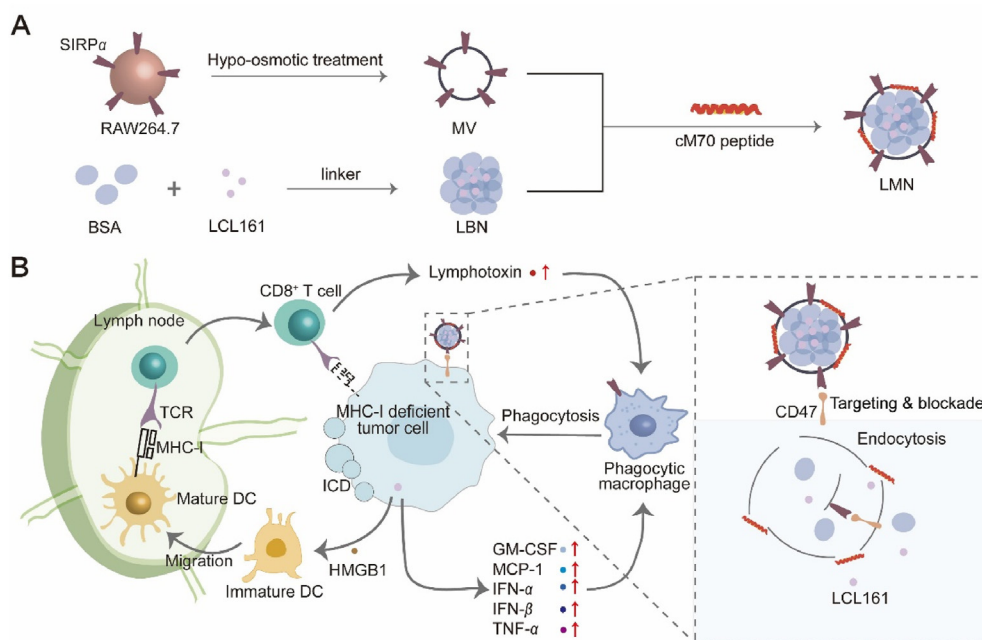
Figure 1 Schematic illustration of the preparation and mechanism of action of LMNs. (A) Preparation of LMNs. (B) Mechanism of action of LMNs. After intravenous injection, LMNs are expected to recognize and enter tumor cells through ligation between CD47 and SIRPα, which can also block CD47-mediated phagocytosis inhibition. LCL161 in LMNs will be released within the cells and is expected to upregulate the expression of various cytokines such as interferon-α (IFN-α), IFN-β, tumor necrosis factor-alpha (TNF-α), granulocyte-macrophage colony-stimulating factor (GM-CSF) and monocyte chemotactic protein 1 (MCP-1) that may activate macrophages. LCL161 can also induce ICD and promote DC maturation, which will enhance CD8$^+$ T cell-mediated release of lymphotoxin that can promote phagocytosis.

cells that cannot be recognized by CD8$^+$ T cells. Therefore, our LMNs are expected to be a useful composite of cancer immunotherapy.

2. Materials and methods

2.1. Reagents

LCL161 was purchased from Shanghai Tebo Chemical Technology Co., Ltd. (Shanghai, China). Macrolittin 70 (M70, NH_2-GIGEVLKELATLLPELQSWIKAAQQL-OH, >98%) was synthesized by Shanghai Top-peptide Biotechnology (Shanghai China). Bovine serum albumin (BSA), FITC-BSA, and Cy5 were purchased from Dalian Meilun Biotechnology Co., Ltd. (Dalian China). RPMI 1640 and Dulbecco's modified Eagle's medium (DMEM) were obtained from Shanghai Yuanpei Biotechnology Co., Ltd., (Shanghai, China). Trypsin, fetal bovine serum (FBS), RAPI lysate, BCA protein assay kit, SDS-PAGE loading buffer, and protein markers were acquired from New Cell & Molecular Biotech Co., Ltd. (Suzhou, China). DAPI was obtained from Yeasen (Shanghai, China). Enzyme-linked immunosorbent assay (ELISA) kits for interleukin-8 (IL8), IL6, GM-CSF, IL12p40, MCP-1, IFN-α, IFN-β were obtained from Neobioscience (Shenzhen, China) and kit for IFN-γ, TNF-α were obtained from Dakewei (Shenzhen, China). Other chemicals were purchased from Sinopharm Chemical Reagent Co., Ltd. (Shanghai, China) unless otherwise indicated.

2.2. Cell and animals

The murine TNBC cell line 4T1 and the macrophage cell line RAW264.7 (derived from BALB/c mice) were purchased from the

Cell Bank of Shanghai, Chinese Academy of Sciences (Shanghai, China). The 4T1$^{H-2Kb\ KO}$ was established from 4T1 using CRISPR-Cas9 genome editing. 4T1 and 4T1$^{H-2Kb\ KO}$ were cultured in RPMI 1640 containing 10% FBS, 1% antibiotics, 2.5 g/L glucose, and 0.11 g/L sodium pyruvate. RAW264.7 was cultured in DMEM containing 10% FBS, and 1% antibiotics. The cells were maintained in a 37 °C incubator containing 5% CO_2. Female BALB/c mice (20−22 g) and female BALB/c nude mice (20−22 g) were purchased from the Shanghai Experimental Animal Center (Shanghai, China). Mice bearing orthotopic 4T1 or 4T1$^{H-2Kb\ KO}$ tumors were established by injecting 100 μL of cancer cell suspension (1 × 10^6 cells) into the third right mammary glands of female BALB/c mice. Animals were kept at 23 °C with standard food and water in a 12-h and 12-h light−dark cycle. All animal procedures were performed according to the guidelines approved by the Institutional Animal Care and Use Committee of the Shanghai Institute of Materia Medica, Chinese Academy of Sciences (2021-06-LYP-43, 2022-06-LYP-44, 2023-07-LYP-45).

2.3. Antibodies

The fluorescence-labeled primary antibodies used for immunostaining were against mouse CD45 (Biolegend, San Diego, CA, USA, cat. no. 103128), mouse CD3 (Biolegend, cat. no. 100328), mouse CD8 (Biolegend, cat. no. 100712), mouse CD11c (Biolegend, cat. no. 117305), mouse MHC-II (Biolegend, cat. no. 107625, cat. no. 107607), mouse CD80 (Biolegend, cat. no. 104707), mouse CD86 (Biolegend, cat. no. 105011), mouse CD11b (Biolegend, cat. no. 101205), mouse F4/80 (Biolegend, cat. no. 123116), mouse Ly6c (Biolegend, cat. no. 128011). The stained cells were detected by a BD Fortessa flow cytometer (BD Biosciences, Franklin Lakes, NJ, USA) and the results were

analyzed with FlowJo software. Primary antibodies used for Western blotting were against SIRPα (Abcam, Cambridge Technology Park, UK, cat. no. ab191419) and CD47 (Affinity, Melbourne, AU, cat. no. DF6649). The secondary antibody used for Western blotting was horseradish peroxidase-labelled goat-anti-rabbit IgG (H + L) (Yeasen, cat. no. 33101ES60). The fluorescence-labeled primary antibodies used for the detection of proteins on cells were against mouse CD47 (Biolegend cat. no. 103127), and mouse SIRPα (Invitrogen, Waltham, MA, USA, cat. no. 2702145). Anti-PD1, anti-PDL1, and anti-CD8 antibodies for the *in vivo* efficacy study were purchased from BioXCell (West Lebanon, NH, USA, cat. no. 29F.1A12, clone: BE0273; cat. no. BE0101, clone: 10F.9G2; cat. no. BE0061, clone: 2.43, respectively).

2.4. Protein expression quantification

The protein expression was quantified using flow cytometry. For the *in vitro* experiment, $4T1^{H-2Kb \; KO}$ cells (2×10^5 cells/well) and RAW264.7 cells (2×10^5 cells/well) were seeded into a 24-well plate for 12 h and then were collected and labeled with fluorescent antibody against mouse CD47 and mouse SIRPα before flow cytometry analysis. For the *in vivo* experiment, $4T1^{H-2Kb \; KO}$ tumor-bearing mice were established as above. Tumors were collected and digested to obtain cell suspensions. For macrophage analysis, cells were incubated with fluorescent antibodies against mouse CD45, mouse F4/80, mouse SIRPα, and mouse CD47. For tumor cell analysis, cells were incubated with antibodies against Epcam, mouse SIRPα, and mouse CD47. All samples were prepared according to the manufacturer's protocols.

2.5. Preparation of membrane vesicles

Macrophage-derived vesicles (MVs) and red blood cell (RBC) vesicles (RVs) were prepared from RAW264.7 cells and RBCs (derived from BALB/c mice), respectively. Briefly, RAW264.7 cells or RBCs were collected after PBS washing, and the cells were resuspended with cold Tris buffer (PH 7.4 with $1 \times$ EDTA-free protease inhibitors) and placed at 4 °C for 2 h. Subsequently, the suspension was centrifuged at $800 \times g$ for 10 min and at $10,000 \times g$ for 10 min (H2050R, Xiangyi, Changsha, China). The supernatants were further centrifuged at $150,000 \times g$ for 1 h (Himac CS GXII, Hitachi, Tokyo, Japan). The obtained cell membrane pellets were resuspended with 10 mM Tris buffer and sonicated with an ultrasonicator (JYD-650L, Zhixin Inc., Shanghai, China) for 30 s. The supernatants were then sequentially extruded through 200 nm and 100 nm polycarbonate membranes with LF-1 (Avastin, Canada) to give MVs and RVs.

2.6. Preparation of LCL161-loaded bovine serum albumin nanoparticles (LBNs)

The LBNs were prepared according to a previous method[40]. Briefly, 25 mg BSA was dissolved in 5 mL of PBS and 3 mg LCL161 was dissolved in 15 mL of anhydrous ethanol. Anhydrous ethanol containing LCL161 was added dropwise to the BSA solution stirred for 30 min, and then incubated at 75 °C for 40 min. The ethanol was removed through evaporation and ultrafiltration to give the LBN solution. FITC-labeled LBNs were prepared using the same method, during which FITC-labeled BSA was used instead of plain BSA. BSA nanoparticles (BNs) without LCL161 were prepared using the same method.

2.7. Preparation of membrane-coated nanoparticles

LBNs (2 mg/mL, 1 mL) were mixed with either MVs or RVs (derived from 2×10^7 cells, 100 μL), followed by a 3 min sonication (4 °C). The prepared nanoparticles were incubated with 7 μL M70 at 4 °C for 30 min and purified by ultrafiltration (100 kDa) to remove free M70. The obtained LMNs or LCL161-loaded RNs (LRNs) were stored in PBS at 4 °C. The content of LCL161 was determined by high-performance liquid chromatography (HPLC, UltiMate 3000, ThermoScientific, USA). The hydrodynamic sizes and ζ-potentials of the nanoparticles were measured using a ZetaSizer (ZS90, Marven Panalytical, Shanghai, China). The morphologies of all the nanoparticles were examined by transmission electron microscopy (TEM, Tecnai G2 F20, FEI, Hillsboro, OR, USA). Nanoparticles without M70 modification were prepared using the same method, except no M70 was used. LCL161-free nanoparticles including macrophage membrane-coated BNs (MNs) and RBC membrane-coated BNs (RNs) were prepared using the same protocol.

2.8. Fluorescence resonance energy transfer (FRET)

The emission spectra of Cy5-labeled MVs/RVs and Cy3-labeled LBNs were collected at their respective excitation wavelengths. The emission spectra of dual-labeled LMNs/LRNs and a mixture of Cy5-labeled MVs/RVs and Cy3-labeled LBNs were collected at an excitation wavelength of 540 nm.

2.9. Cellular uptake

$4T1^{H-2Kb \; KO}$ cells (5×10^4 cells/well) were seeded into a 24-well plate stayed for 12 h, and then incubated with FITC-labeled nanoparticles for 1 or 4 h before flow cytometry analysis. To compare the cellular uptake of LMNs and anti-CD47 antibodies on RBC and $4T1^{H-2Kb \; KO}$ cells, FITC-labeled LMNs or anti-CD47 were added, and the cells were collected and analyzed by flow cytometry at 4 h after administration.

2.10. Cellular colocalization in vitro and in vivo

To observe the subcellular location of the nanoparticles, the nanoparticles were fluorescently labeled with FITC in the cores and with Cy5 in the membrane. $4T1^{H-2Kb \; KO}$ cells (5×10^4 cells/well) were seeded into a 24-well plate with cell slides and placed for 12 h and then were incubated with the fluorescent-labeled nanoparticles for 1 or 4 h. The cells were then fixed, and stained with DAPI, Lysotracker Red, and anti-CD47 antibodies to visualize nuclei, lysosomes, and CD47, respectively, before being imaged on a confocal laser scanning microscopy (TCS SP8, Leica, Wetzlar, GER). For the *in vivo* experiments, tumor-bearing mice were treated with dual-labeled LMNs for 4 h before harvesting the tumors. The tissues were fixed, sliced, and stained before being imaged using confocal laser scanning microscopy (TCS SP8, Leica).

2.11. Phagocytosis and BMDC maturation in vitro

$4T1^{H-2Kb \; KO}$ cells (5×10^4 cells/well) were seeded into a 24-well plate for 12 h. The cells were treated with LMN, LRN, LBN, LPS, or PBS for 18 h before another 24 h of coincubation with BMDC (2×10^5 cells/well). Cells were collected, stained with antibodies against mouse CD11c, mouse CD86, and mouse CD80, and

further analyzed by flow cytometry. For the phagocytosis experiment, the treated 4T1$^{H-2Kb\ KO}$ cells were stained with CFSE for 10 min before incubation with BMDM (2×10^5 cells/well) for 24 h. The cells were then collected, stained with antibodies against mouse F4/80 and mouse CD11b, and further analyzed by flow cytometry.

2.12. Biodistribution

Mice bearing orthotopic 4T1$^{H-2Kb\ KO}$ tumors (around 100 mm^3) were established as described above, and randomly assigned to different groups to receive Cy5-labeled LMN, LRN, or LBN. Mice were imaged using an IVIS Spectrum imaging system ($\lambda_{Ex}/\lambda_{Em} = 650/670$ nm, PerkinElmer, MA, USA) at 1, 2, 4, 8, 12, and 24 h after administration. In a separate experiment, mice were sacrificed by CO$_2$ asphyxiation at 4 h and 24 h and the major organs were collected for imaging. At 4 h after the injection, major organs and tumors were collected and weighed. LCL161 in the major organs and tumors were extracted with acetonitrile and quantified by liquid chromatography-mass spectrometry (LC−MS, QTRAP$^®$ 5500 triple quadrupole tandem mass spectrometer, Sciex, USA).

2.13. Cytokines detection

4T1$^{H-2Kb\ KO}$ cells (5×10^4 cells/well) were seeded into a 24-well plate and attached for 12 h before incubating with fresh medium containing LMN, LRN, LBN, or PBS for another 18 h. The amounts of MCP-1, IL8, GM-CSF, IFN-α, IFN-β, and TNF-α in the medium were measured using ELISA kits according to the manufacturer's protocols. To determine the amounts of cytokines *in vivo*, tumor-bearing mice were first established as described above. Serum, draining lymph nodes (DLNs), and tumors were collected on Day 5 after the last injection of a 4-dose or 7-dose regime. Lymph nodes and tumors were weighed, ground, and finally centrifuged to collect supernatants. The levels of IL8, GM-CSF, MCP-1, lymphotoxin, IL12p40, IFN-γ, and TNF-α in the samples were measured using ELISA kits according to the manufacturer's protocols. The biochemical indicators alanine aminotransferase (ALT), aspartate aminotransferase (AST), creatinine (CREA), and blood urea nitrogen (UREA) were sent out to the Wuhan Servicebio Technology Co., Ltd. for analysis.

2.14. Antitumor immunity

The 4T1$^{H-2Kb\ KO}$ tumor-bearing mice models were established as above. When the size of tumors reached ~ 30 mm^3, the mice were randomly grouped to receive LMN, LRN, LBN, anti-PD1, or PBS (anti-PD1: i.p., 50 μL, 50 μg per mouse, 3 times once a week; nanoparticles: i.v., 100 μL, 10 mg/kg in LCL161, once every 3 days for 7 times). Mice were sacrificed by carbon dioxide asphyxiation on Day 5 after the last administration, and the tumors and DLNs were collected to obtain cell suspensions. Cells were counted with a cell counter and then incubated with antibodies against mouse CD45, mouse CD3, and mouse CD8. For macrophage analysis, cells were incubated with antibodies against mouse CD45, mouse CD11b, mouse F4/80, mouse MHC-II, and mouse Ly6c. For DCs analysis, cells were incubated with antibodies against mouse CD45, mouse CD11c, mouse MHC-II, mouse CD80, and CD86. All samples were prepared according to the manufacturer's protocols and analyzed by flow cytometry (BD Biosciences).

2.15. Antitumor efficacy

Tumor-bearing mice were established as described above. When the size of the tumor reached ~ 30 mm^3, the mice were randomly assigned to different groups to receive LMN, LRN, LBN, anti-PD1 or PBS (anti-PD1: i.p., 50 μL, 50 μg per mouse for 3 times once a week; nanoparticles: i.v., 100 μL, 10 mg/kg in LCL161, once every 3 days for 7 times). Body weight and tumor volume were measured every 2 days. To understand the role of CD8$^+$ T cells in the treatment of MHC-I deficient tumors, we depleted CD8$^+$ T cells using the corresponding antibodies in some mice. Mice received CD8 depleting antibody or IgG isotype (100 μg per mouse) on the day of tumor inoculation and then every 3 days until euthanasia, and received LMN or PBS (i.v., 10 mg/kg in LCL161, once every 3 days).

2.16. Statistics

Statistical analysis of the data was performed using Prism 9.5 (GraphPad software). Data were analyzed with a two-sided Student's *t*-test when two groups were compared. One-way ANOVA was used when more than two groups were analyzed. Tumor growth profiles were analyzed by two-way ANOVA. The survival benefit was determined using a log-rank test. *$P < 0.05$, **$P < 0.01$, ***$P < 0.001$, and ****$P < 0.0001$ were considered as statistically significant.

3. Results

3.1. Efficacy of macrophage-derived nanoparticles and LCL161 against 4T1$^{H-2Kb\ KO}$ tumor

Our previous study has shown that 4T1$^{H-2Kb\ KO}$ tumors are resistant to CTL-mediated immune clearance due to β2M gene deletion[25]. However, the growth of 4T1$^{H-2Kb\ KO}$ tumors could be moderately retarded after interferon supplementary therapy, indicating a potential role of innate immunity in tumor control. Since CD47/SIRPα is an important immune checkpoint for macrophage-mediated antitumor immunity, we tested the potential of SIRPα-displaying nanoparticles in tumor growth inhibition. First, we compared the expression of CD47 and SIRPα by 4T1$^{H-2Kb\ KO}$ cells and macrophages. Western blot analysis showed that 4T1$^{H-2Kb\ KO}$ cells expressed CD47 but not SIRPα, while RAW264.7 cells, in sharp contrast, expressed SIRPα but low CD47 (Fig. 2A), which results were further quantitatively confirmed by flow cytometry (Supporting Information Fig. S1). Based on this finding, MNs were prepared and used to treat 4T1$^{H-2Kb\ KO}$ tumors. Tumor growth was retarded by 43% in mice receiving MNs but not in those receiving PBS, BNs, or RNs (Fig. 2B and C), and no significant loss of body weight was observed (Supporting Information Fig. S2). These results suggest that competitive blocking of CD47/SIRPα interaction can improve antitumor immunity against TNBC tumors with MHC-I-related gene loss.

LCL161 has been reported to promote antitumor immunity independent of MHC-I expression in murine models of colon cancer or pancreatic cancer[16]. To explore whether LCL161 would be effective in treating 4T1$^{H-2Kb\ KO}$ tumors, we injected LCL161 intratumorally and monitored tumor growth. LCL161 inhibited the growth of 4T1$^{H-2Kb\ KO}$ tumors, and tumor burden was reduced by 42% compared to those receiving PBS (Fig. 2D and E). Furthermore, we explored changes in the major effector cells after LCL161 treatment. The flow cytometry result revealed that
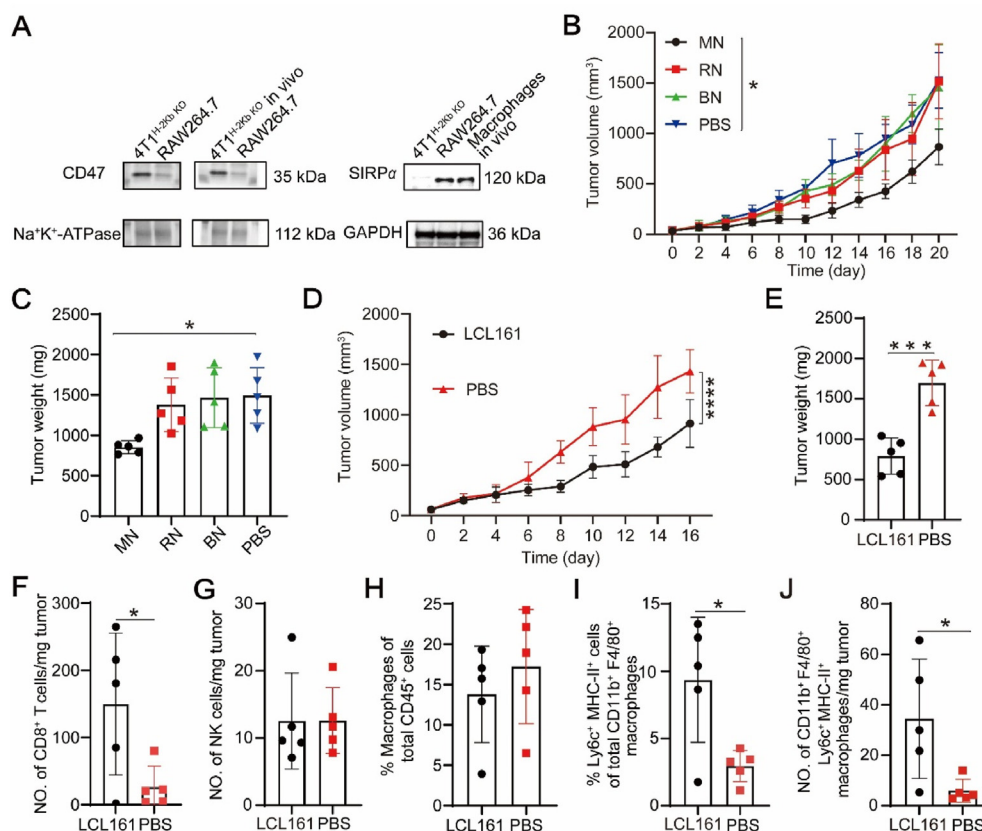
Figure 2 Efficacy of MNs and LCL161 in $4T1^{H-2Kb\ KO}$ tumors. (A) Western blot analysis of the expression of CD47 and SIRPα proteins in $4T1^{H-2Kb\ KO}$, RAW264.7, and macrophages. (B, C) Growth profiles (B) and weights (C) of $4T1^{H-2Kb\ KO}$ tumors from mice receiving the indicated treatments (i.v., $n = 5$). (D, E) Growth profiles (D) and weights (E) of $4T1^{H-2Kb\ KO}$ tumors from mice receiving the indicated treatments (LCL161: i.t., 10 μL, 30 μg per mouse, $n = 5$). (F–J) Intratumoral densities of CD8$^+$ T cells (F) and NK cells (G), percentage of macrophages among total immune cells (H), percentage of phagocytic macrophage subtype among macrophages (I), and intratumoral density of phagocytic macrophage subtype (J) in $4T1^{H-2Kb\ KO}$ tumors after different treatments. Data are presented as mean $\pm$ SD and statistical significance was calculated using a two-sided two-way ANOVA test (for B and D), a one-way ANOVA test (C), and a Student's t-test (E–J), respectively. *$P < 0.05$, **$P < 0.01$, ***$P < 0.001$ and ****$P < 0.0001$.

LCL161 increased the density of intratumoral CD8$^+$ T cells (Fig. 2F) but not NK cells (Fig. 2G). Although the proportion of macrophages among immune cells (CD45$^+$) did not increase (Fig. 2H), the proportion (Fig. 2I) and the density (Fig. 2J) of phagocytic macrophage subtype (CD11b$^+$F4/80$^+$Ly6c$^+$MHC-II$^+$) increased. These results indicated that LCL161 mainly affected CTLs and macrophages. Since $4T1^{H-2Kb\ KO}$ cells could not present peptide-MHC-I complexes that were essential for CTL-mediated cell therapy, the increased CTLs could play a role in potentiating macrophage-mediated cancer cell eradication. As MNs and LCL161 both showed significant but moderate antitumor efficacy through different mechanisms of action, combination use of the two treatments could be beneficial.

3.2. Preparation and characterization of LMNs

MN and LCL161 could be combined in LMNs by loading LCL161 into the core of MN. LBNs were prepared using a previously reported method[40]. The LBNs were then coated with cell membranes derived from either RAW264.7 or RBC and were further decorated with cM70 (an activatable peptide that could be anchored to cell membranes by covalent attachment and resume its membrane rupture activity after exposure to glutathione

(GSH)[25,41], Supporting Information Figs. S3–S6) to obtain LMNs and LRNs, respectively. The nanoparticles were purified through ultrafiltration to remove free drugs. Transmission electron microscopy (TEM) images revealed that both LMNs and LRNs were spherical particles with a lightly stained core, which were usually disrupted by the water-soaked core nanogel under vacuum, while the LBNs were heavily stained with uranyl acetate due to their nature as nanogels (Fig. 3A and Supporting Information Fig. S7). To further verify the structures of LMNs and LRNs, LBNs and cell membrane vesicles were labeled with Cy3 and Cy5, respectively. Significant fluorescence resonance energy transfer (FRET) was observed in LMNs and LRNs but not in the mixtures of membrane vesicles and LBNs, further confirming the successful formation of the core-shelled structures (Fig. 3B). Dynamic light scattering analysis showed that both LMNs and LRNs were around 150 nm in diameter with ζ-potentials around −25 mV (Fig. 3C), which were stable for at least 72 h (Fig. 3D). The obtained LMN and LRN each contained 39 and 33 cM70 molecules on average, respectively. Further gel electrophoresis and Western blot analysis confirmed that the characteristic proteins were well retained in the LMNs and LRNs during the preparation (Fig. 3E). The drug loading capacity and drug encapsulation efficiency were $8.5 \pm 0.2\%$ and $59.7 \pm 1.6\%$ for LMN and $8.1 \pm 0.6\%$ and
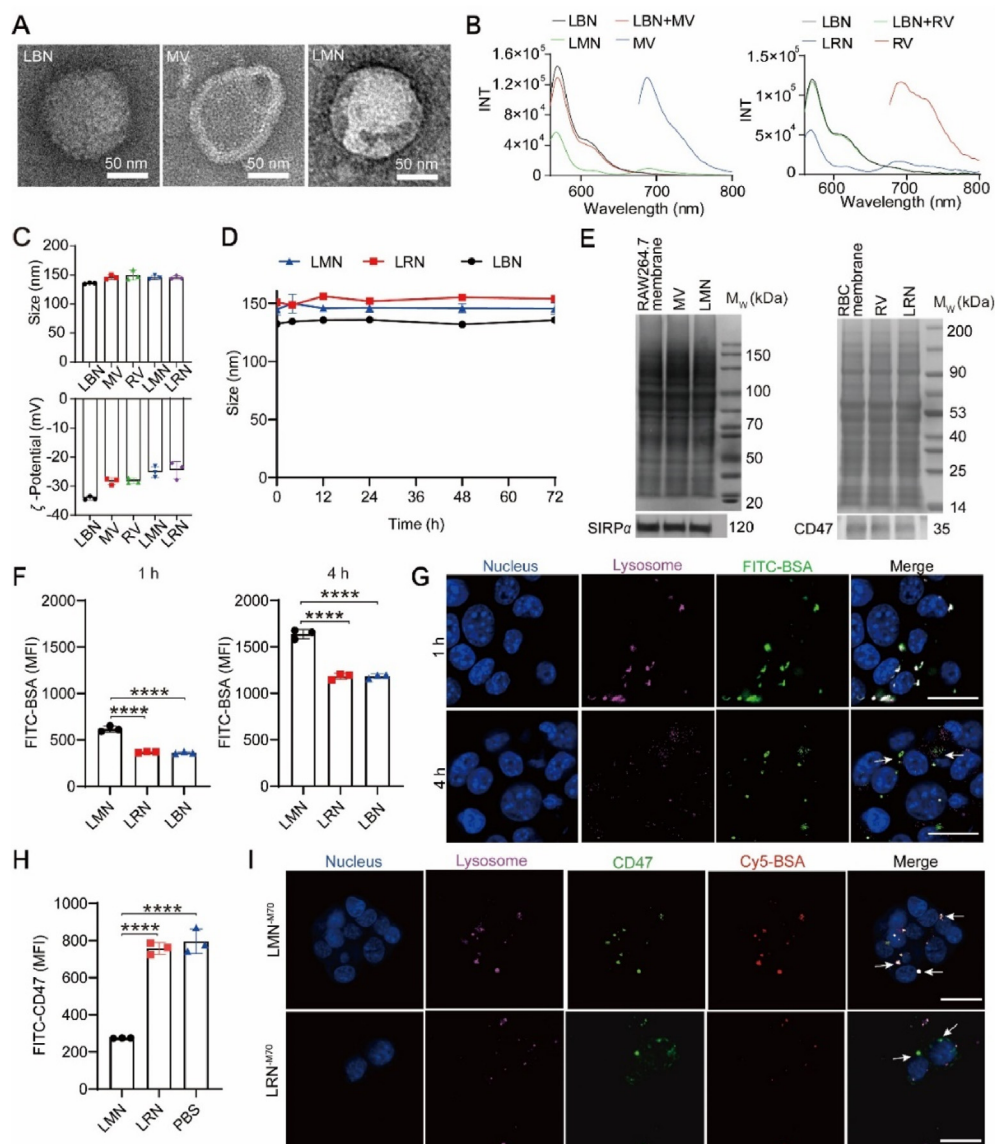
Figure 3 Characterization and cellular uptake of LMNs. (A) TEM images of the LBN, MV, and LMN. (B) Fluorescent spectra of LMN/LRN, LBN, MV/RV, and a mixture of LBN and MV/RV (LBN + MV/RV). The BSA was labeled with Cy3, and the MV/RV was labeled with Cy5. The emission spectra of LMN/LRN, LBN, and LBN + MV/RV were collected under excitation at 540 nm. The emission spectrum of MV/RV was collected under excitation at 650 nm. FRET occurs only in LMN/LRN. (C) Hydrodynamic sizes and ζ-potentials of different particles. (D) Stability of LMN, LRN, and LBN over 72 h. (E) SDS-PAGE and Western blot analysis of SIRPα protein on the RAW264.7 membrane, MV and LMN, and of the CD47 protein on the RBC membrane, RV and LRN. (F) Cellular uptake of LMN, LRN, and LBN (with FITC-labeled BSA) by 4T1$^{\text{H-2Kb KO}}$ cells after 1 or 4 h of incubation. (G) Representative confocal images showing the intracellular localization of FITC-labeled BSA. The nucleus was stained with DAPI (blue). The scale bar indicates a distance of 25 μm. (H) Flow cytometry determination of CD47 on the surface of 4T1$^{\text{H-2Kb KO}}$ after 4 h of co-incubation with the indicated nanoparticles. (I) Representative confocal images showing cellular localization of CD47, lysosomes, and indicated nanoparticles in 4T1$^{\text{H-2Kb KO}}$ cells. Data are presented as mean ± SD ($n = 3$) and statistically analyzed using a two-sided one-way ANOVA test. *$P < 0.05$, **$P < 0.01$, ***$P < 0.001$ and ****$P < 0.0001$.

56.1 ± 4.1% for LRN, respectively. The encapsulated LCL161 was stably trapped in the nanoparticles but could be abruptly released from the nanoparticles after exposure to GSH (Supporting Information Fig. S8).

We then explored the interaction of LMNs with 4T1$^{\text{H-2Kb KO}}$ cells *in vitro*. To quantify and visualize the LMNs, we labeled the albumin with FITC, as we previously reported. Flow cytometry analysis revealed a higher cellular uptake of LMNs than LRNs and LBNs at 1 and 4 h after treatments (Fig. 3F). Further confocal

images showed that LMNs and LRNs would undergo endocytosis and colocalize with lysosomes within 1 h after incubation with cancer cells. After 4 h of incubation, diffusive FITC-albumin signals could be observed in both LMNs and LRNs treated cells, most of which did not colocalize with lysosomes (Fig. 3G and Supporting Information Fig. S9). Furthermore, we investigated the influence of nanoparticles on cell surface CD47. Flow cytometry analysis revealed that the amount of surface CD47 was reduced by 65% after a 4 h-incubation with LMN$^{-\text{M70}}$

(LMNs without cM70), while no significant change was noticed in cells incubated with LRN^{-M70} (LRNs without cM70) (Fig. 3H). Confocal images showed that CD47 molecules were intracellularly colocalized with lysosomes and LMN^{-M70}, while the CD47 signal was mainly observed on the cell membrane of cells treated with LRN^{-M70} (Fig. 3I). These results demonstrate that LMNs can enter cells with CD47 and release their encapsulated contents into the cytosol after a short colocalization with the lysosomes, indicating that LMNs can be a cancer cell-targeted vehicle and a CD47 blocker.

3.3. Antitumor immunity in vitro

Encouraged by the above results, we first investigated the effects of LMNs on 4T1$^{H-2Kb\ KO}$ cells. ELISA showed that the concentrations of various cytokines such as GM-CSF, MCP-1, IL8, TNF-α, IFN-α, and IFN-β in the medium of the LMNs-treated tumor cells were significantly increased, while LRNs and LBNs were less effective (Fig. 4A). Additionally, a 47% increase in the concentration of the high mobility group protein 1 (HMGB1) was observed after LMN treatment, indicating that some cancer cells had undergone ICD (Fig. 4B). These results suggested that LMNs could induce damage to cancer cells, which would further trigger immune responses.

Given that LCL161 could increase intratumoral densities of both CTLs and macrophages, we investigated the immune priming activity of LMNs on both bone marrow-derived DCs (BMDCs) and bone marrow-derived macrophages (BMDMs) (Fig. 4C). Flow cytometry analysis showed that the maturation rates of BMDCs (CD80$^+$CD86$^+$) were 55.9%, 51.0%, 38.4% and 33.3% when they were incubated with 4T1$^{H-2Kb\ KO}$ cells that were pretreated with LMNs, LRNs, LBNs and PBS, respectively (Fig. 4D and E). In consistency, the highest concentrations of pro-inflammatory factors including TNF-α, IL12p40, and IFN-γ were detected in those pretreated with LMNs (Fig. 4F).

We then explored the capability of LMNs in priming BMDM and explored the impact of LMNs on the phagocytosis of tumor cells by macrophages. The results demonstrated that LMNs promoted the polarization of BMDM into phagocytic macrophage subtype and also improved macrophage phagocytosis capability (Fig. 4G and Supporting Information Fig. S10). In consistency, elevated concentrations of GM-CSF, IL6, and TNF-α were recorded after the same treatment, confirming phagocytic macrophage activation (Fig. 4H). The results show that tumor cell-secreted cytokines promoted DC maturation and macrophage polarization, while activated macrophages and DCs further promoted cytokine secretion. The results demonstrate that the increase in tumor cell phagocytosis by macrophages could be because LCL161 promoted cancer cell secretion of inflammatory factors that stimulated the polarization of the phagocytic macrophage subtype.

3.4. Biodistribution and biocompatibility

As we discussed above, CD47 was also expressed on the surface of erythrocytes[42]. Thus, we first compared the selectivity of LMNs between 4T1$^{H-2Kb\ KO}$ cells and RBCs before the in vivo study. In a mixture of 4T1$^{H-2Kb\ KO}$ cells and RBCs, LMNs mainly targeted cancer cells while the anti-CD47 antibody showed a higher affinity for erythrocytes (Fig. 5A and B). Based on this result, we investigated the tissue distribution of LMNs, LRNs, and LBNs using an IVIS Spectrum Imaging System

($\lambda_{Ex}/\lambda_{Em}$ = 650/670 nm). Maximum tumor accumulation of the nanoparticles was achieved 4 h after intravenous injection, with prolonged tumor retention observed only in LMNs (Fig. 5C and D). Confocal imaging confirmed a higher intratumoral accumulation of LMNs (Fig. 5E) and further revealed that the BSA would be liberated from the macrophage membrane shell (Fig. 5F). To directly monitor drug distribution, the intratumoral accumulation of LCL161 at 4 h after the injection of different nanoparticles was quantified by LC$-$MS. The intratumoral concentration of LCL161 in LMNs-treated mice was 0.8- and 1.0-fold higher than those in mice receiving LRN and LBN, respectively (Fig. 5G). Although all nanoparticles showed a high liver accumulation, no significant differences were observed in serum ALT and AST among mice that received different treatments (Fig. 5H) as well as CREA and blood UREA (Supporting Information Fig. S11). In consistency, no obvious tissue damage was observed in the major organs, except for mild leukocyte infiltration in the lungs collected from the PBS and LBN groups (Supporting Information Fig. S12). The inflammation might be associated with tumor burden-induced formation of premetastatic niches in the lungs, which were the main destination of metastatic TNBC[43]. These results demonstrated that LMNs were efficient in tumor-targeted drug delivery largely due to specific recognition between SIRPα and CD47 molecules. Although CD47 molecules were expressed both on cancer cells and RBCs, the preferential accumulation of LMNs in 4T1$^{H-2Kb\ KO}$ cells could be associated with multivalent recognition-induced endocytosis, which was common in cancer cells but not in RBCs. Antibodies with high affinity for CD47 may be inefficient in triggering endocytosis, and thus mainly targeted RBCs.

3.5. Antitumor immunity in vivo

We then investigated the efficacy of LMNs in modulating antitumor immunity. In consistence with the in vitro results, intratumoral concentrations of MCP-1, GM-CSF, TNF-α, and IL8 increased significantly in tumors of mice receiving nanoparticles but not in those receiving anti-PD1 antibodies or PBS (Fig. 6A$-$E). Flow cytometry analysis further revealed that the proportion of phagocytic macrophage subtype (CD11b$^+$F4/80$^+$MHC-II$^+$Ly6c$^+$) among macrophages in tumors was significantly increased by LMNs and LRNs (Fig. 6F and Supporting Information Fig. S20A), although the proportion of macrophages (CD11b$^+$F4/80$^+$) among immune cells (CD45$^+$) was not affected (Supporting Information Fig. S13). The density of the phagocytic macrophage subtype was increased by 15-fold and 6-fold by LMNs and LRNs, respectively (Fig. 6G). These results indicated that LCL161 was essential in promoting the secretion of inflammatory cytokines by 4T1$^{H-2Kb\ KO}$ tumors[44]. These cytokines promoted the macrophage polarization into phagocytic macrophage subtypes. LMN might also act as a multivalent blocker of CD47 on the surface of tumor cells and thus would aid the phagocytic macrophage subtype.

Given that BMDC could be activated by LMNs in vitro, we expected that LMNs would promote DC maturation in vivo. Indeed, ELISA analysis showed that LMNs also induced ICD in tumors (Supporting Information Fig. S14), which was coincident with significant increases in the density of intratumoral mature DCs by 10-fold (Fig. 6H and Fig. S20B), the percentage of mature DCs in DLNs by 1-fold (Fig. 6I), and inflammatory cytokines (TNF-α, IL12p40 and IFN-γ) in the DLNs (Fig. 6J). LMNs also increased the density of intratumoral CD8$^+$ T cells (Fig. 6K) and
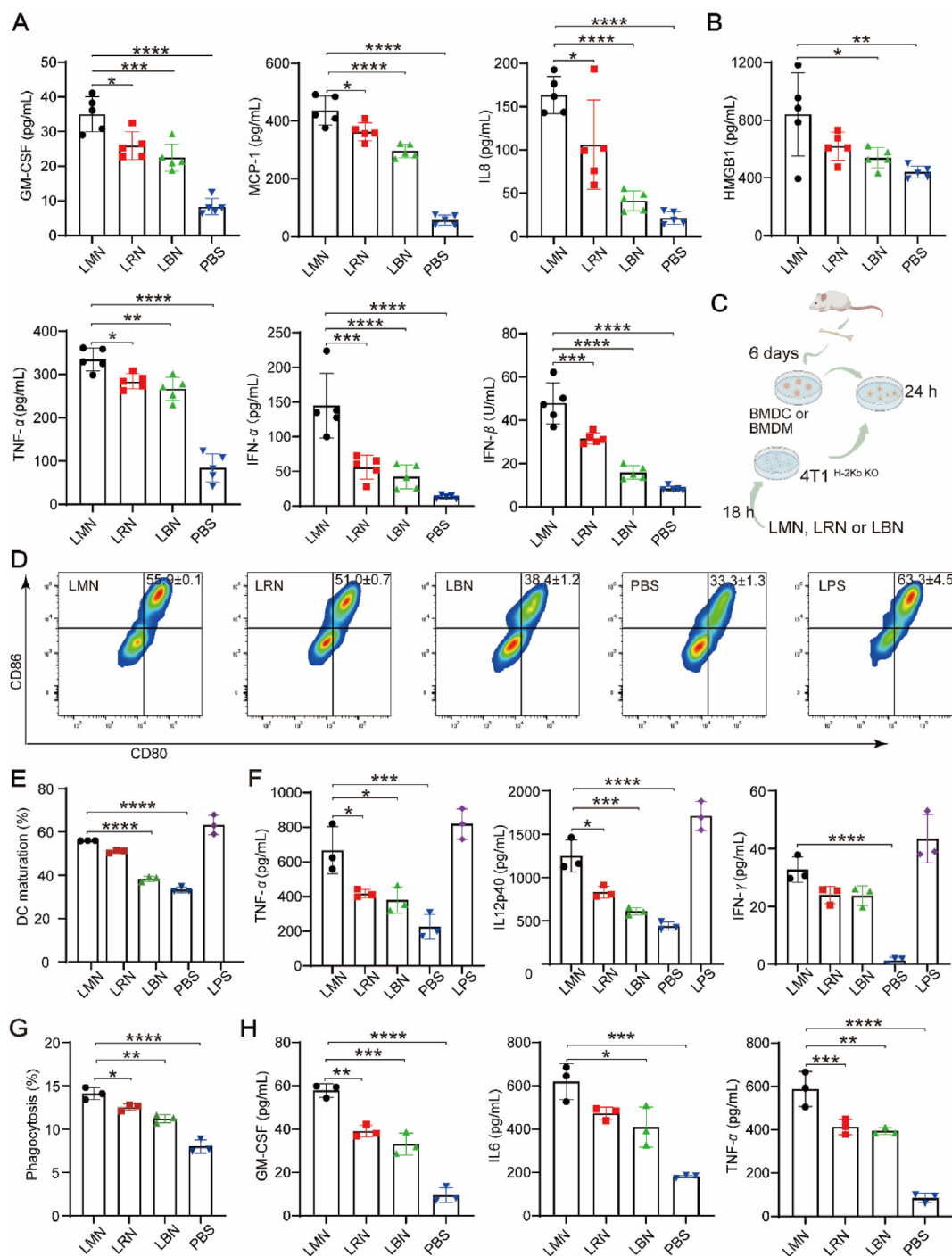
Figure 4 Activity of LMNs *in vitro*. (A) Qualification of the secreted GM-CSF, MCP-1, IL8, TNF-α, IFN-α, and IFN-β in mediums of 4T1$^{H-2Kb\ KO}$ cells after different treatments. (B) Quantification of extracellular HMGB1 in the medium of 4T1$^{H-2Kb\ KO}$ cells after different treatments. (C) Schematic illustration of experimental procedures for BMDC and BMDM maturation studies *in vitro*. The figure was created with permission from BioRender.com. (D−F) Flow cytometry plots (D) and quantification (E) of mature BMDCs (CD80$^+$CD86$^+$), and concentrations of TNF-α, IL12p40, and IFN-γ in the medium (F) after a 24 h-incubation with 4T1$^{H-2Kb\ KO}$ cells that were pretreated with different nanoparticles. BMDCs treated with PBS or LPS were used as controls. (G) Flow cytometry analysis of phagocytosis of 4T1$^{H-2Kb\ KO}$ by BMDM. (H) Concentrations of GM-CSF, IL6, and TNF-α in the coculture of BMDM and treated 4T1$^{H-2Kb\ KO}$. Data are presented as mean $\pm$ SD ($n = 3$) and statistical significance was calculated using a two-sided one-way ANOVA test. *$P < 0.05$, **$P < 0.01$, ***$P < 0.001$ and ****$P < 0.0001$.

the amount of intratumoral lymphotoxin (Fig. 6L), but the percentages of proliferative (Ki-67$^+$) and active (GzmB$^+$) CTLs among all CTLs did not increase (Supporting Information Figs. S15 and Fig. S20C). This was not a surprise, since CTL

activation required recognition between the neoantigen-bound MHC−I complex in cancer cells and the T-cell receptor (TCR) in CTLs[45]. However, since lymphotoxin from CD8$^+$ T cells was able to stimulate macrophage transformation[16], increased
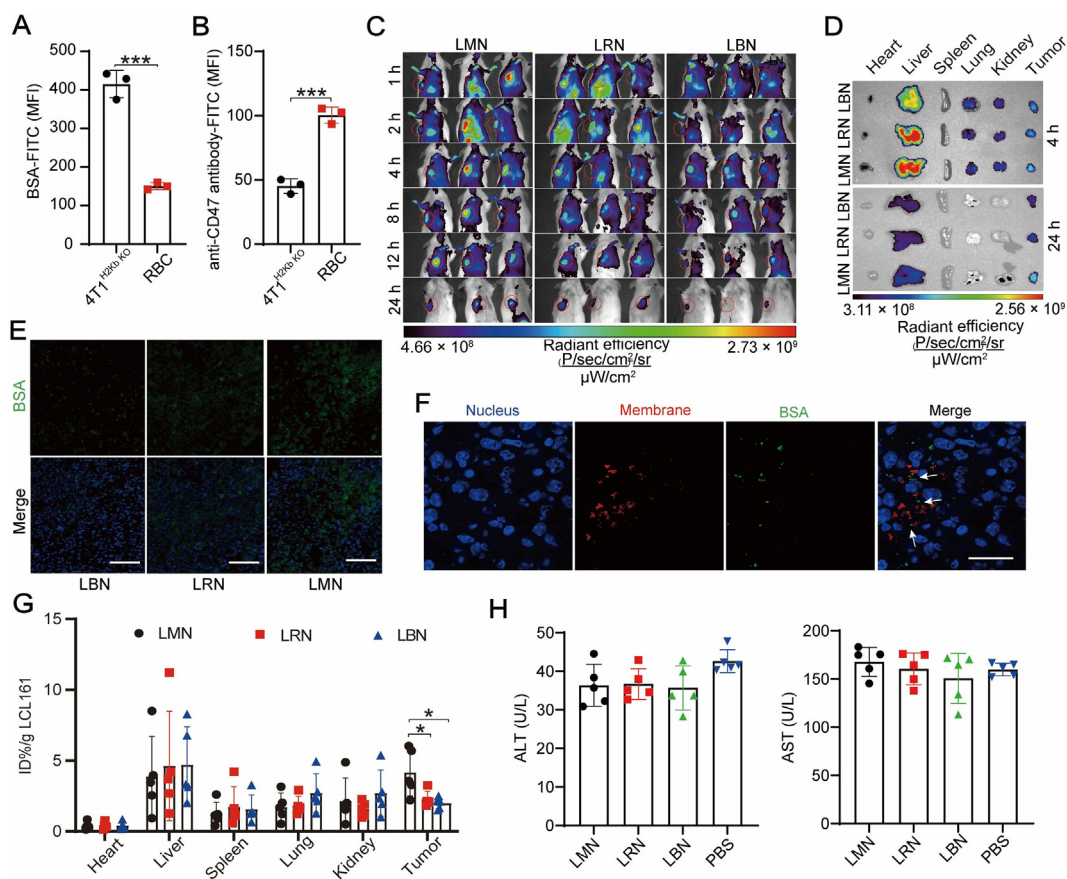
Figure 5 Accumulation and biocompatibility of LMNs. (A, B) Cellular uptake of FITC-labeled BSA in LMNs (A) and FITC-labeled anti-CD47 antibody (B) by 4T1$^{H-2Kb\ KO}$ cells or erythrocytes after 4 h of incubation ($n = 3$). Data were statistically analyzed using a two-sided Student's t-test. (C, D) Fluorescence images of mice at 1, 2, 4, 8, 12, and 24 h after injection (C) and images of the major organs at 4 and 24 h after injection (D). These mice were injected with Cy5-labeled LBNs, LRNs, or LMNs (Cy5: 0.1 mg/kg, i.t.), and imaged by an IVIS Spectral Imaging System ($\lambda_{Ex}/\lambda_{Em} = 650/670$ nm). (E) Fluorescent images of tumor slices collected from mice at 4 h after different treatments. The LBNs, LRNs, and LMNs were labeled with FITC, and the nucleus was labeled with DAPI (blue). The scale bar indicates 200 μm. (F) Confocal images showing the location of the FITC-labeled BSA and the Cy5-labeled membrane of nanoparticles. The nucleus was stained with DAPI (blue). The scale bar indicates 50 μm. (G) The distribution of LCL161 in major organs and tumors at 4 h after injection of LMNs, LRNs, and LBNs (LCL161: 10 mg/kg, $n = 5$). (H) Serum levels of ALT and AST at 5 days after the last injection of a 4-injection regime of LMNs, LRNs, and LBNs (20 mg/kg in LCL161) ($n = 5$). Data are expressed as mean ± SD and statistical significance was calculated using a two-sided one-way ANOVA test. *$P < 0.05$, **$P < 0.01$, ***$P < 0.001$ and ****$P < 0.0001$.

intratumoral density of CTLs could work synergistically with phagocytic macrophage subtype and also contribute to antitumor immunity against MHC-I-deficient tumors. The above results demonstrated that LMNs promoted the release of inflammatory cytokines, which activated macrophages and increased tumor cell phagocytosis. Meanwhile, SIRPα on the LMNs (as CD47 blockers) and lymphotoxins released by CD8$^+$ T cells could further enhance macrophage phagocytic activity (Fig. 6M).

3.6. Efficacy of LMNs against 4T1$^{H-2Kb\ KO}$ murine TNBC tumors

We evaluated the efficacy of LMNs in mice with orthotopic 4T1$^{H-2Kb\ KO}$ tumors. Tumor growth was retarded by 86.7% after seven doses of LMNs, while LRN and LBN showed tumor inhibition of 59.6% and 48.4% (Fig. 7A and B). Tumor weights in LMNs-treated mice were only 17.6% of those in PBS-treated mice at the end of the study (Fig. 7C), without causing a noticeable

decrease in body weight (Supporting Information Fig. S16). Further immunofluorescence analysis of tumors revealed that only LMNs negatively regulated CD47 tumor expression (Supporting Information Fig. S17). Besides, the median survival time (MST) of mice was extended from 22 days (PBS group) to 48, 29, and 28 days by LMNs, LRNs, and LBNs, respectively (Fig. 7D and Supporting Information Fig. S18). On the contrary, anti-PD1 antibodies did not show significant tumor growth inhibition activity. These results demonstrated that LMNs could effectively inhibit MHC-I-deficient tumors, which were resistant to current PDL1/PD1 blockade therapy.

To better understand the role of CTLs in LMNs-mediated antitumor efficacy. We also tested the tumor suppression efficacy of LMNs in immunodeficient mice. We found that LMNs could inhibit the growth of 4T1$^{H-2Kb\ KO}$ tumors in nude mice (inhibition rate 41.6%) but much less compared to immunocompetent mice (Fig. 7E). In a separate experiment, anti-CD8 antibodies were used in combination with LMNs to treat immunocompetent mice that bearing 4T1$^{H-2Kb\ KO}$ tumors. A sharp decrease in the
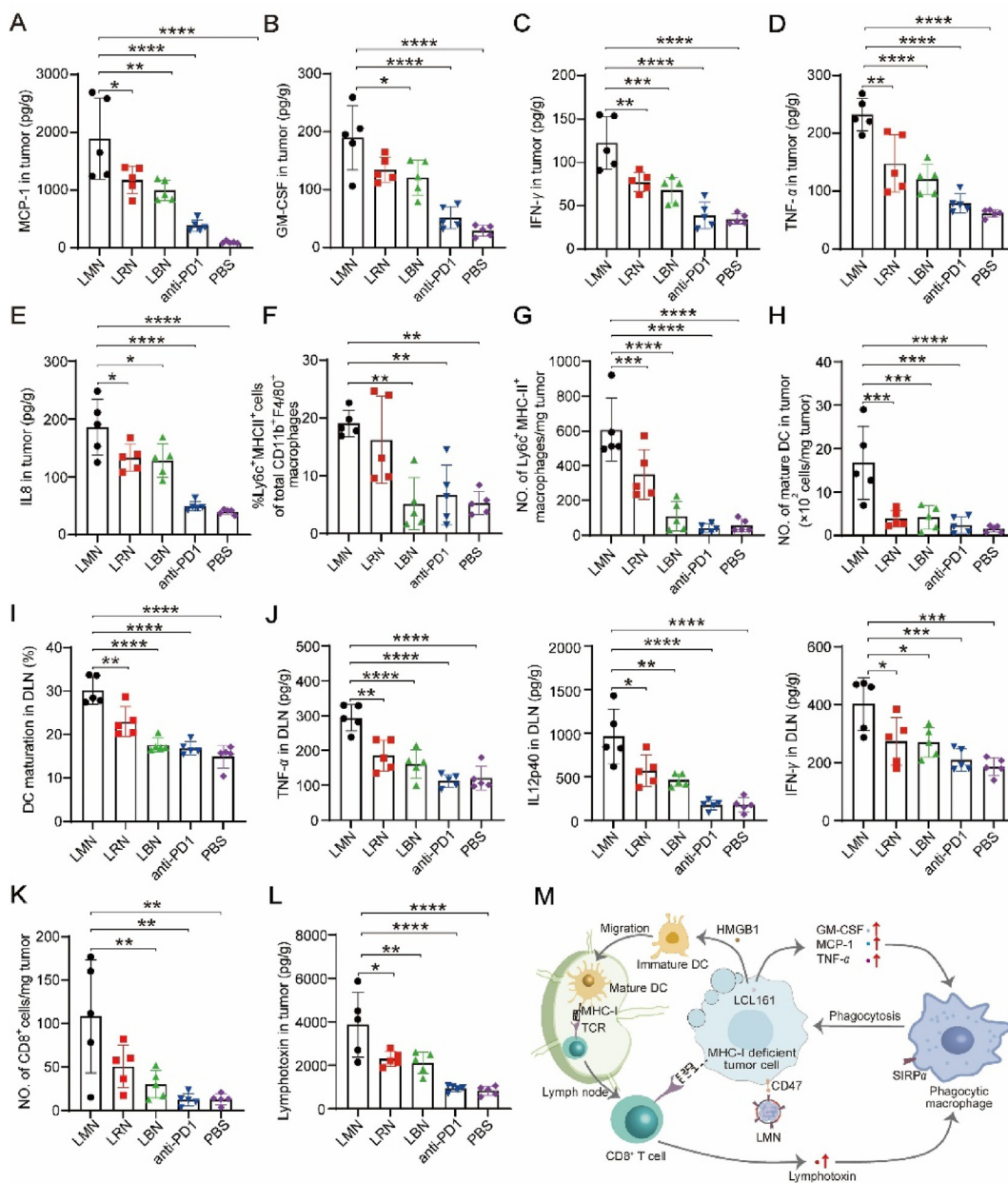
Figure 6 Antitumor immunity *in vivo*. (A–E) Qualification of the secreted MCP-1 (A), GM-CSF (B), IFN-γ (C), TNF-α (D), and IL8 (E) in tumors collected on Day 5 after a 4-dose regime (LCL161: 10 mg/kg, ani-PD1: 50 μg per mouse, once every 3 days). (F–H) Percentage (F) and density (G) of phagocytic macrophage subtype (Ly6c$^+$ MHC-II$^+$), and density of matured DCs (H) in the tumors collected from mice on Day 5 after a 7-dose regime (LCL161: 10 mg/kg, ani-PD1: 50 μg per mouse, once every 3 days). (I–L) Percentage of mature DCs (I) and concentrations of cytokines (TNF-α, IL12p40, and IFN-γ) (J) in DLNs, density of CD8$^+$ T cells (K) and concentration of lymphotoxin (L) in the tumors collected from mice on Day 5 after a 7-dose regime (LCL161: 10 mg/kg, ani-PD1: 50 μg per mouse, once every 3 days). (M) Proposed mechanisms of action of LMNs. Data are presented as mean ± SD ($n = 5$) and statistical significance was calculated using a two-sided one-way ANOVA test. *$P < 0.05$, **$P < 0.01$, ***$P < 0.001$ and ****$P < 0.0001$.

antitumor activity of LMNs was observed when used in conjunction with anti-CD8 antibodies, while control IgG showed no effect on the efficacy of LMNs (Fig. 7F and G). These results suggested that CTLs also played an important role in macrophage-mediated antitumor immunity, possibly by secreting lymphotoxins that could potentiate the phagocytic macrophage subtype.

Finally, we tested the efficacy of LMNs on TNBC tumors that were resistant to combined chemotherapy and anti-PDL1 immunotherapy. The 4T1 tumor that responded poorly to the

combinatorial therapy was cut and transplanted to the mammary fat pads of naïve mice (Supporting Information Fig. S19). In mice bearing pretreated 4T1 tumors, LMNs inhibited tumor growth by 71.8%, while the growth inhibition rate of combined therapy with albumin-bound paclitaxel and anti-PDL1 antibodies was 50.2% (Fig. 7H). In consistency, the MST of mice was extended from 14 days (PBS group) to 28 days (Fig. 7I). These results demonstrated that LMNs might be used to treat refractory TNBC that had undergone current combination therapy.
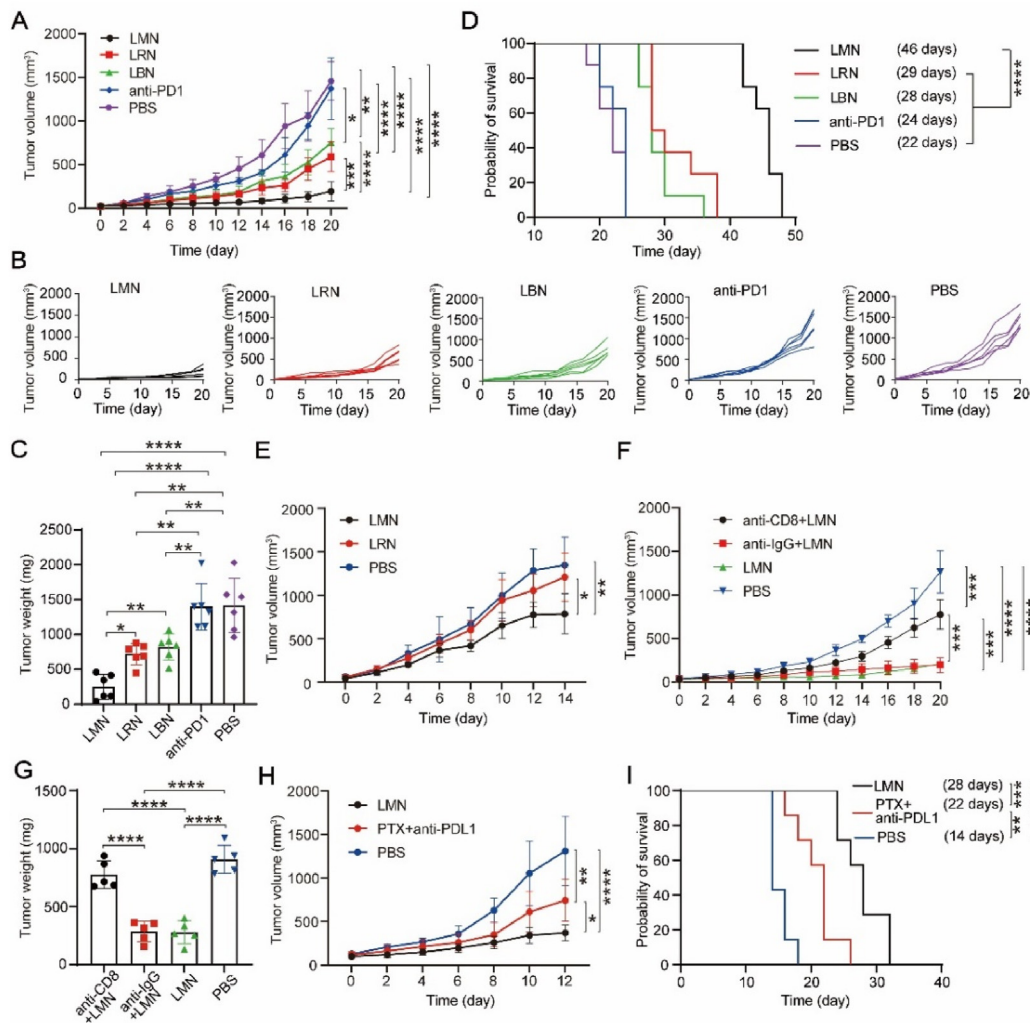
Figure 7 Antitumor efficacy of LMNs. (A−D) Growth profiles of 4T1$^{H-2Kb\ KO}$ tumors ($n = 6$) (A, B), the tumor weight (C), and survival curves ($n = 8$) (D) of mice receiving the indicated treatments (i.v., LCL161: 10 mg/kg once every 3 days, anti-PD1: 50 μg per mouse once a week). (E) Growth profiles of 4T1$^{H-2Kb\ KO}$ tumors of nude mice receiving the indicated treatments (LCL161: 10 mg/kg, $n = 5$). (F, G) Growth profiles of 4T1$^{H-2Kb\ KO}$ tumors (F) and tumor weight (G) of the mice receiving the indicated treatments. Mice received depleting antibodies on the day of tumor inoculation and then once every 3 days until euthanasia. (LCL161: 10 mg/kg, i.v., anti-CD8: 100 μg per mouse, i.p., $n = 5$). (H, I) Growth profiles of treatment-resistant 4T1 tumors (H) and survival curves (I) of mice receiving the indicated treatments (LCL161: 10 mg/kg, PTX: 6 mg/kg, $n = 7$). Data are presented as the mean ± SD. Tumor growth data were analyzed by two-way ANOVA and survival data by log-rank test. Tumor weight data were analyzed by two-sided one-way ANOVA. *$P < 0.05$, **$P < 0.01$, ***$P < 0.001$ and ****$P < 0.0001$.

4. Discussions

The efficacy of current cancer immunotherapy is highly dependent on intratumoral infiltration of CTLs and the expression of MHC-I molecules on cancer cells[46]. Combination use of chemotherapy with current immunotherapy can improve CTL infiltration[47]. However, MHC-I-deficient tumors that are commonly observed in patients with TNBC are refractory to treatment[48,49]. In our previous study, TNBC cancer with epigenetically downregulated MHC-I could be effectively treated using an epigenetic nanoparticle, which however was ineffective against 4T1$^{H-2Kb\ KO}$ tumors[25].

Innate immune cells such as macrophages can eradicate MHC-I-deficient cancer cells, but the efficacy is limited by an insufficient amount of phagocytic macrophage subtype and CD47-mediated activity blockade. Hence, we demonstrate a strategy to promote macrophage-based innate antitumor immunity by creating an LCL161-loaded and macrophage membrane-coated

nanoparticle termed LMN for the treatment of TNBC with $\beta2M$ loss. The shell of LMNs is derived from macrophages that naturally express SIRPα, which can target and block CD47 on cancer cells[50,51]. The nanoparticle is used to deliver LCL161, a cIAP1/2 inhibitor[52−54], that can promote the production of inflammatory factors *via* activating nonclassical NF-κB pathway[44,55]. In mice bearing 4T1$^{H-2Kb\ KO}$ tumors, we show that LMNs increase intratumoral levels of inflammatory factors including MCP-1, IL8, GM-CSF, IFN-α, IFN-β, and TNF-α, which elevate the intratumoral density of phagocytic macrophage subtype. LMNs are also effective in treating 4T1 tumors that are resistant to combination therapy with albumin-bound paclitaxel and anti-PDL1 antibodies.

A key hurdle for CD47 blockade therapy is the on-target off-site binding of antibodies to CD47 molecules on RBCs. In our case, although the SIRPα on LMNs is also capable of binding to CD47 in RBCs, the affinity of SIRPα for CD47 (in micromolar

ranges) is almost 1000-fold weaker than that of anti-CD47 antibodies[56]. The relatively lower affinity allows LMNs to detach from RBCs and then relocate to cancer cells. Given that cancer cells typically have a higher level of endocytosis than RBCs with a rigid morphology, we demonstrate that LMNs are preferentially endocytosed by cancer cells. Furthermore, the multivalent nature of LMNs also facilitates endocytosis of surface CD47, which is critical to blocking the "don't eat me" signal on cancer cells.

Successful antitumor immunity induction requires effective communication between innate and adaptive immune cells. Although 4T1$^{\text{H-2Kb KO}}$ cells lack β2M expression, DC-mediated antigen presentation, and CTL activation are still functional. Although these CTLs cannot recognize MHC-I-deficient cancer cells, they can still be recruited to the tumor and activated by mature DCs in the tumors. These CTLs are important participants in LMN-primed antitumor immunity, as the efficacy of LMNs decreased after CD8$^+$ T cells depletion or in nude mice. We demonstrate that the CTLs can enhance the activity of the phagocytic macrophage subtype by secreting lymphotoxin.

5. Conclusions

We have demonstrated the efficacy of LMN in 4T1$^{\text{H-2Kb KO}}$ model mice, immunodeficient mice, and model mice with tumor progression after combinatorial treatment with PTX and anti-PDL1. Our mechanistic study reveals that both innate and adaptive immune cells contribute to the efficacy of LMNs. Therefore, we envision that the treatment can further benefit from combination therapy. For the future clinical translation of the platform, personalized LMNs prepared from patient-derived macrophages are preferred to minimize potential immunogenicity. However, genetically modified macrophages can be further explored to produce generalizable and multifunctional LMNs. Given the advances in techniques in genetic manipulation cell expansion and quality control, we believe that our LMNs will find broad applications, especially in patients with recurrent diseases after current immunotherapy.

Author contributions

Wen Zhang and Pengcheng Zhang conceived and designed the project; Wen Zhang, Yihui Zhai, Ying Cai, Xiang Gong, Yunxuan Jiang, Rong Rong, Chao Zheng and Binyu Zhu performed the cell and animal experiments; Wen Zhang and Pengcheng Zhang interpreted the data and wrote the original manuscript; Pengcheng Zhang, Helen He Zhu, Hao Wang, and Yaping Li revised the manuscript; all authors edited the manuscript; Pengcheng Zhang, Hao Wang, and Yaping Li supervised the project.

Conflicts of interest

The authors have no conflicts of interest to declare.

Appendix A.   Supporting information

Supporting information to this article can be found online at https://doi.org/10.1016/j.apsb.2024.04.009.

References

1. Roemer MGM, Advani RH, Ligon AH, Natkunam Y, Redd RA, Homer H, et al. PD-L1 and PD-L2 genetic alterations define classical hodgkin lymphoma and predict outcome. *J Clin Oncol* 2016;**34**: 2690−7.
2. Stenzel PJ, Schindeldecker M, Tagscherer KE, Foersch S, Herpel E, Hohenfellner M, et al. Prognostic and predictive value of tumor-infiltrating leukocytes and of immune checkpoint molecules PD1 and PDL1 in clear cell renal cell carcinoma. *Transl Oncol* 2020;**13**: 336−45.
3. Kumar S, Chatterjee M, Ghosh P, Ganguly KK, Basu M, Ghosh MK. Targeting PD-1/PD-L1 in cancer immunotherapy: an effective strategy for treatment of triple-negative breast cancer (TNBC) patients. *Genes Dis* 2023;**10**:1318−50.
4. Doroshow DB, Bhalla S, Beasley MB, Sholl LM, Kerr KM, Gnjatic S, et al. PD-L1 as a biomarker of response to immune-checkpoint inhibitors. *Nat Rev Clin Oncol* 2021;**18**:345−62.
5. Thacker G, Henry S, Nandi A, Debnath R, Singh S, Nayak A, et al. Immature natural killer cells promote progression of triple-negative breast cancer. *Sci Transl Med* 2023;**15**:eabl4414.
6. Christine MM, Paul LC, Lucas AH, Kristin CH, Claudia P, Jeffrey S, et al. Tumor-targeted interleukin-12 synergizes with entinostat to overcome PD-1/PD-L1 blockade-resistant tumors harboring MHC-I and APM deficiencies. *JITC* 2022;**10**:e004561.
7. Zhang X, Ge X, Jiang T, Yang R, Li S. Research progress on immunotherapy in triple-negative breast cancer. *Int J Oncol* 2022;**61**: 95.
8. Zheng C, Zhang W, Wang J, Zhai Y, Xiong F, Cai Y, et al. Lenvatinib- and vadimezan-loaded synthetic high-density lipoprotein for combinational immunochemotherapy of metastatic triple-negative breast cancer. *Acta Pharm Sin B* 2022;**12**:3726−38.
9. Bae J, Liu L, Moore C, Hsu E, Zhang A, Ren Z, et al. IL-2 delivery by engineered mesenchymal stem cells re-invigorates CD8$^+$ T cells to overcome immunotherapy resistance in cancer. *Nat Cell Biol* 2022;**24**: 1754−65.
10. Guan Q, Han M, Guo Q, Yan F, Wang M, Ning Q, et al. Strategies to reinvigorate exhausted CD8$^+$ T cells in tumor microenvironment. *Front Immunol* 2023;**14**:1204363.
11. Li Y, Zhang H, Merkher Y, Chen L, Liu N, Leonov S, et al. Recent advances in therapeutic strategies for triple-negative breast cancer. *J Hematol Oncol* 2022;**15**:121.
12. Liu Y, Qiu N, Shen L, Liu Q, Zhang J, Cheng YY, et al. Nanocarrier-mediated immunogenic chemotherapy for triple negative breast cancer. *J Control Release* 2020;**323**:431−41.
13. Zhou Z, Liu Y, Song W, Jiang X, Deng Z, Xiong W, et al. Metabolic reprogramming mediated PD-L1 depression and hypoxia reversion to reactivate tumor therapy. *J Control Release* 2022;**352**:793−812.
14. Zhou Z, Wang H, Li J, Jiang X, Li Z, Shen J. Recent progress, perspectives, and issues of engineered PD-L1 regulation nano-system to better cure tumor: a review. *Int J Biol Macromol* 2024;**254**:127911.
15. Lin W, Chen L, Zhang H, Qiu X, Huang Q, Wan F, et al. Tumor-intrinsic YTHDF1 drives immune evasion and resistance to immune checkpoint inhibitors *via* promoting MHC-I degradation. *Nat Commun* 2023;**14**:265.
16. Roehle K, Qiang L, Ventre KS, Heid D, Ali LR, Lenehan P, et al. cIAP1/2 antagonism eliminates MHC class I−negative tumors through T cell−dependent reprogramming of mononuclear phagocytes. *Sci Transl Med* 2021;**13**:eabf5058.
17. Chen X, Lu Q, Zhou H, Liu J, Nadorp B, Lasry A, et al. A membrane-associated MHC-I inhibitory axis for cancer immune evasion. *Cell* 2023;**186**. 3903-20.e21.

18. Taylor BC, Balko JM. Mechanisms of MHC-I downregulation and role in immunotherapy response. *Front Immunol* 2022;**13**:35296095.

19. Xu Y, Xiong J, Sun X, Gao H. Targeted nanomedicines remodeling immunosuppressive tumor microenvironment for enhanced cancer immunotherapy. *Acta Pharm Sin B* 2022;**12**:4327−47.

20. Fangazio M, Ladewig E, Gomez K, Garcia-Ibanez L, Kumar R, Teruya-Feldstein J, et al. Genetic mechanisms of HLA-I loss and immune escape in diffuse large B cell lymphoma. *Proc Natl Acad Sci U S A* 2021;**118**:e2104504118.

21. McGranahan N, Rosenthal R, Hiley CT, Rowan AJ, Watkins TBK, Wilson GA, et al. Allele-specific HLA loss and immune escape in lung cancer evolution. *Cell* 2017;**171**. 1259-71.e11.

22. Dusenbery AC, Maniaci JL, Hillerson ND, Dill EA, Bullock TN, Mills AM. MHC class I loss in triple-negative breast cancer: a potential barrier to PD-1/PD-L1 checkpoint inhibitors. *Am J Surg Pathol* 2021;**45**:701−7.

23. Montesion M, Murugesan K, Jin DX, Sharaf R, Sanchez N, Guria A, et al. Somatic HLA class I loss is a widespread mechanism of immune evasion which refines the use of tumor mutational burden as a biomarker of checkpoint inhibitor response. *Cancer Discov* 2021;**11**:282−92.

24. Taylor BC, Sun X, Gonzalez-Ericsson PI, Sanchez V, Sanders ME, Wescott EC, et al. NKG2A is a therapeutic vulnerability in immunotherapy resistant MHC-I heterogeneous triple negative breast cancer. *Cancer Discov* 2023:1−18.

25. Zhai Y, Wang J, Lang T, Kong Y, Rong R, Cai Y, et al. T lymphocyte membrane-decorated epigenetic nanoinducer of interferons for cancer immunotherapy. *Nat Nanotechnol* 2021;**16**:1271−80.

26. Labanieh L, Majzner RG, Mackall CL. Programming CAR-T cells to kill cancer. *Nat Biomed Eng* 2018;**2**:377−91.

27. Zhang C, Liu J, Zhong JF, Zhang X. Engineering CAR-T cells. *Biomark Res* 2017;**5**:22.

28. Maalej KM, Merhi M, Inchakalody VP, Mestiri S, Alam M, Maccalli C, et al. CAR-cell therapy in the era of solid tumor treatment: current challenges and emerging therapeutic advances. *Mol Cancer* 2023;**22**:20.

29. Nasiri F, Kazemi M, Mirarefin SMJ, Mahboubi Kancha M, Ahmadi Najafabadi M, Salem F, et al. CAR-T cell therapy in triple-negative breast cancer: hunting the invisible devil. *Front Immunol* 2022;**13**:36483567.

30. Barkal AA, Weiskopf K, Kao KS, Gordon SR, Rosental B, Yiu YY, et al. Engagement of MHC class I by the inhibitory receptor LILRB1 suppresses macrophages and is a target of cancer immunotherapy. *Nat Immunol* 2018;**19**:76−84.

31. Liu Q, Li J, Zheng H, Yang S, Hua Y, Huang N, et al. Adoptive cellular immunotherapy for solid neoplasms beyond CAR-T. *Mol Cancer* 2023;**22**:28.

32. Feng M, Jiang W, Kim BYS, Zhang CC, Fu YX, Weissman IL. Phagocytosis checkpoints as new targets for cancer immunotherapy. *Nat Rev Cancer* 2019;**19**:568−86.

33. Liu Ye, Wang Y, Yang Y, Weng L, Wu Q, Zhang J, et al. Emerging phagocytosis checkpoints in cancer immunotherapy. *Signal Transduct Targeted Ther* 2023;**8**:104.

34. Logtenberg MEW, Scheeren FA, Schumacher TN. The CD47-SIRPα immune checkpoint. *Immunity* 2020;**52**:742−52.

35. Yuan J, Shi X, Chen C, He H, Liu L, Wu J, et al. High expression of CD47 in triple negative breast cancer is associated with epithelial-mesenchymal transition and poor prognosis. *Oncol Lett* 2019;**18**:3249−55.

36. Chen C, Wang R, Chen X, Hou Y, Jiang J. Targeting CD47 as a novel immunotherapy for breast cancer. *Front Oncol* 2022;**12**:924740.

37. Dooling LJ, Andrechak JC, Hayes BH, Kadu S, Zhang W, Pan R, et al. Cooperative phagocytosis of solid tumours by macrophages triggers durable anti-tumour responses. *Nat Biomed Eng* 2023;**7**:37095318.

38. Liu R, Luo C, Pang Z, Zhang J, Ruan S, Wu M, et al. Advances of nanoparticles as drug delivery systems for disease diagnosis and treatment. *Chin Chem Lett* 2023;**34**:107518.

39. Varfolomeev E, Blankenship JW, Wayson SM, Fedorova AV, Kayagaki N, Garg P, et al. IAP antagonists induce autoubiquitination of c-IAPs, NF-κB activation, and TNFα-dependent apoptosis. *Cell* 2007;**131**:669−81.

40. Steinhauser IM, Langer K, Strebhardt KM, Spänkuch B. Effect of trastuzumab-modified antisense oligonucleotide-loaded human serum albumin nanoparticles prepared by heat denaturation. *Biomaterials* 2008;**29**:4022−8.

41. Grasso G, Muscat S, Rebella M, Morbiducci U, Audenino A, Danani A, et al. Cell penetrating peptide modulation of membrane biomechanics by Molecular dynamics. *J Biomech* 2018;**73**:137−44.

42. Burger P, Hilarius-Stokman P, de Korte D, van den Berg TK, van Bruggen R. CD47 functions as a molecular switch for erythrocyte phagocytosis. *Blood* 2012;**119**:5512−21.

43. Liu Y, Cao X. Characteristics and significance of the pre-metastatic niche. *Cancer Cell* 2016;**30**:668−81.

44. Chesi M, Mirza NN, Garbitt VM, Sharik ME, Dueck AC, Asmann YW, et al. IAP antagonists induce anti-tumor immunity in multiple myeloma. *Nat Med* 2016;**22**:1411−20.

45. Taylor B, Balko J, Sanders M, Gonzalez-Ericsson P, Sanchez V. 318 Enforced tumor specific MHC-I heterogeneity in triple negative breast cancer drives immunotherapy resistance. *J Immunotherapy Cancer* 2021;**9**:A342.

46. Wang Y, Wang X, Cui X, Zhuo Y, Li H, Ha C, et al. Oncoprotein SND1 hijacks nascent MHC-I heavy chain to ER-associated degradation, leading to impaired CD8⁺ T cell response in tumor. *Sci Adv* 2020;**6**:eaba5412.

47. Wang S, Zhou Z, Hu R, Dong M, Zhou X, Ren S, et al. Metabolic intervention liposome boosted lung cancer radio-immunotherapy *via* hypoxia amelioration and PD-L1 restraint. *Adv Sci* 2023;**10**:e2207608.

48. Haugh A, Daud A. Resistance to immune checkpoint blockade: IFNγ or MHC-I?. *Cancer Immunol Res* 2023;**11**:864.

49. Gu SS, Zhang W, Wang X, Jiang P, Traugh N, Li Z, et al. Therapeutically increasing MHC-I expression potentiates immune checkpoint blockade. *Cancer Discov* 2021;**11**:1524−41.

50. Kim YK, Hong Y, Bae YR, Goo J, Kim SA, Choi Y, et al. Advantage of extracellular vesicles in hindering the CD47 signal for cancer immunotherapy. *J Control Release* 2022;**351**:727−38.

51. Choi Y, Nam G-H, Kim GB, Kim S, Kim YK, Kim SA, et al. Nanocages displaying SIRP gamma clusters combined with prophagocytic stimulus of phagocytes potentiate anti-tumor immunity. *Cancer Gene Ther* 2021;**28**:960−70.

52. Chesi M, Garbitt V, Palmer S, Bergsagel PL. IAP antagonists are a novel class of immunomodulators that induce complete response in Vk*MYC myeloma by stimulating plasmacytoid dendritic cells to secrete IFNa. *Blood* 2013;**122**:128.

53. Gu JJ, Mavis C, Torka P, Sundaram S, Hernandez-Ilizaliturri FJ. Potentiate immune activation and function by targeting inhibitor of apoptosis proteins (IAPs) in relapse/refractory DLBCL. *Blood* 2020;**136**:30−1.

54. Yang C, Wang H, Zhang B, Chen Y, Zhang Y, Sun X, et al. LCL161 increases paclitaxel-induced apoptosis by degrading cIAP1 and cIAP2 in NSCLC. *J Exp Clin Cancer Res* 2016;**35**:158.

55. Koch PD, Rodell CB, Kohler RH, Pittet MJ, Weissleder R. Myeloid cell-targeted nanocarriers efficiently inhibit cellular inhibitor of apoptosis for cancer immunotherapy. *Cell Chem Biol* 2020;**27**:94−104.e5.

56. Qu T, Li B, Wang Y. Targeting CD47/SIRPα as a therapeutic strategy, where we are and where we are headed. *Biomark Res* 2022;**10**:20.